Chapter 21

Noise in Classical and Quantum Photon-Correlation Imaging

Bahaa E. A. Saleh and Malvin Carl Teich
Boston University

21.1 Introduction

Imaging is the estimation of the spatial distribution of a physical object by measuring the optical radiation it emits, or by making use of an optical wave that interacts with the object, via reflection or transmission, for example, before being measured by a detector.[1] The resolution of an imaging system is limited by the inability to localize the optical field at points of the object. Under otherwise ideal conditions, resolution is limited by diffraction. The sensitivity of an imaging system is limited by the uncertainty in the measurement. Under ideal conditions, this is determined by photon noise, which depends on the statistical fluctuations of the light.

In conventional imaging systems, an extended detector, such as a CCD camera or an array detector, measures the spatial distribution of the optical intensity, which is proportional to the photon flux density. In interferometric systems, the spatial distribution of the optical field is inferred from measurements of the optical intensity. [2]

With the emergence of coherence theory,[2–5] imaging systems based on measurements of the second-order coherence function at pairs of points in the detection plane were developed. An example is the imaging of an incoherent object based on the van Cittert-Zernike theorem. Imaging systems based on measurement of intensity correlation, or the photon coincidence rate, at pairs of points, were developed in the 1960s. A classic example of the photon-correlation imaging of an object emitting thermal light is stellar imaging using a Hanbury-Brown–Twiss intensity-correlation interferometer.[4–7]

More recently, two-photon light, which may be generated via spontaneous parametric downconversion in a second-order nonlinear optical crystal,[8] has been used for imaging.[9–17] This type of two-photon (or biphoton) imaging, which has come to be called quantum imaging, is also based on the measurement of photon coincidence by the use of photon-counting array detectors or by scanning two photon-counting detectors at pairs of points.

To compare the resolution and sensitivity of imaging systems based on the aforementioned types of measurements, it is necessary to derive expressions for the measured quantities in terms of the object distribution. The point-spread functions based on such expressions can be used to assess the resolution. One measure of the sensitivity of the imaging process is the signal-to-noise ratio (SNR) of the measured variables. The statistical nature of the light source must be known in order to determine the SNR.[1,5]

The purpose of this chapter is to compare the resolution and sensitivity of photon-correlation imaging systems that make use of thermal light and two-photon light. We will henceforth refer to these two imaging modalities as classical and quantum photon-correlation imaging, or simply classical and quantum imaging, respectively. Clearly, light in other quantum states can also be used for imaging.

21.2 Classical Photon-Correlation Imaging

Consider the imaging system shown schematically in Fig. 21.1. The source emits quasi-monochromatic, spatially incoherent light with intensity $I_s(\mathbf{x})$, where $\mathbf{x} = (x, y)$. The emitted light reaches the two detectors via two linear systems with impulse response functions $h_1(\mathbf{x}_1, \mathbf{x})$ and $h_2(\mathbf{x}_1, \mathbf{x})$. The object may reside in either of these systems, or in the source itself. The two systems may also be combined as one system in which the object resides.

Based on coherence theory and a systems description of the imaging process,[2,18,] the second-order coherence function $G^{(1)}(\mathbf{x}_1, \mathbf{x}_2) = \left\langle E^*(\mathbf{x}_1)E(\mathbf{x}_2) \right\rangle$ is related to the source intensity and the impulse response functions by the integral,
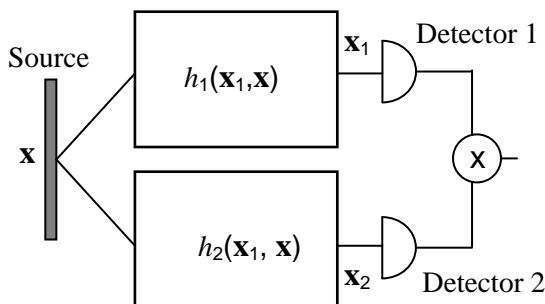
Figure 21.1 Imaging system.

$$G^{(1)}(\mathbf{x}_1,\mathbf{x}_2) = \int \acute{Z} I_s(\mathbf{x}) h_1^*(\mathbf{x}_1,\mathbf{x}) h_2(\mathbf{x}_2,\mathbf{x}) \acute{Z} d\mathbf{x} \,. \tag{21.1}$$

The range of the integrals is [-∞, ∞] throughout, unless otherwise indicated.

21.2.1 Ghost imaging

If the object resides in the first system and has a complex amplitude transmittance (or reflectance) $O(\mathbf{x})$, then $h_1(\mathbf{x}_1,\mathbf{x})$ is linearly related to $O(\mathbf{x})$. Consequently, if $G^{(1)}(x_1,x_2)$ is measured as a function of $\mathbf{x}_1$ with $\mathbf{x}_2$ fixed, the measurement would be linearly related to $O(\mathbf{x})$ so that the imaging system is coherent [i.e., it measures the complex amplitude transmittance (or reflectance)]. For example, consider an object placed in one branch of the system at a distance d_1 from the source, with a lens used to collect the transmitted light and focus it onto detector 1. The other branch of the system contains a lens of focal length f placed in the space between the source and detector 2 at distances d_2 and d_3, as shown in Fig. 21.2. For such a system, Eq. (21.1) leads to diffraction-limited imaging if the focusing condition

$$\frac{1}{d_2 - d_1} + \frac{1}{d_3} = \frac{1}{f} \tag{21.2}$$

is satisfied. This type of imaging is peculiar since the light field that is transmitted through the object is collected and observed with a point detector at the fixed point $\mathbf{x}_2$. The image is acquired by scanning detector 1 at all points $\mathbf{x}_1$ and by observing the light that has not interacted with the object. This type of image may be dubbed ghost imaging, although that appellation historically originated in the context of quantum imaging.
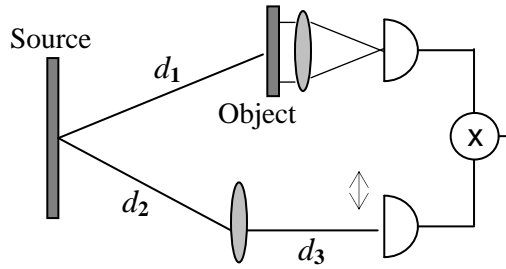
Figure 21.2 Ghost-imaging system.

21.2.2 Van Cittert–Zernike theorem

As another example, assume that the object itself is the source, i.e., $O(\mathbf{x}) = I_s(\mathbf{x})$, and assume that the two systems are combined into a single 2-*f* optical system, as shown in Fig. 21.3, whereupon

$$h_1(\mathbf{x}_1, \mathbf{x}) = h_2(\mathbf{x}_1, \mathbf{x}) \propto \exp\left(-i\frac{2\pi}{\lambda f}\mathbf{x}_1 \cdot \acute{\mathbf{x}}\right), \tag{21.3}$$

Where λ is the wavelength of the light and *f* is the focal length of the lens. In this case, Eq. (21.1) provides

$$G^{(1)}(\mathbf{x}_1, \mathbf{x}_2) \propto \int O(\mathbf{x})\exp\left[-i\frac{2\pi}{\lambda f}(\mathbf{x}_2 - \mathbf{x}_1)\cdot\acute{\mathbf{x}}\right]\acute{d}\mathbf{x}. \tag{21.4}$$

When measured as a function of the position difference $\mathbf{x}_1 - \mathbf{x}_2$, the coherence function $G^{(1)}$ is proportional to the Fourier transform of $O(\mathbf{x})$. Equation (21.4) is the van Cittert–Zernike theorem and is the basis of a well-known technique for measuring the angular diameter of stars.[2–6]
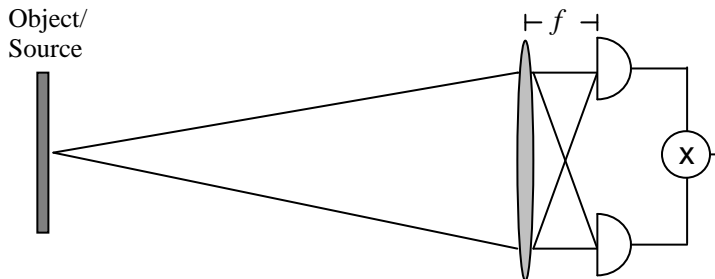

Figure 21.3 Photon-correlation imaging of the source.

21.2.3 Hanbury-Brown-Twiss interferometer

The intensity-correlation function, which is a special fourth-order coherence function,[18] at the positions $\mathbf{x}_1$ and $\mathbf{x}_2$ is $G^{(2)}(\mathbf{x}_1,\mathbf{x}_2) = \langle I_1(\mathbf{x}_1)I_2(\mathbf{x}_2)\rangle$. If the incoherent light is thermal (which at one time was called chaotic), the rate of photon coincidence is related to the second-order coherence function by the Siegert relation,[5]

$$G^{(2)}(\mathbf{x}_1,\mathbf{x}_2) = G^{(1)}(\mathbf{x}_1,\mathbf{x}_1)G^{(1)}(\mathbf{x}_2,\mathbf{x}_2) + \frac{1}{M}\left|G^{(1)}(\mathbf{x}_1,\mathbf{x}_2)\right|^2, \qquad (21.5)$$

where $M \geq 1$ is a factor (known as the degrees of freedom) that increases with increase of the ratio of the detector response time to the optical coherence time. This equation is the basis of the Hanbury-Brown-Twiss effect.[4–7] Thus, the measurement of the intensity-correlation function $G^{(2)}(\mathbf{x}_1,\mathbf{x}_2)$ and the intensity at $G^{(1)}(\mathbf{x},\mathbf{x})$ at all points permit the magnitude of the second-order coherence function to be determined. This principle has served as the basis of a number of schemes for ghost imaging with thermal light.[19–22] A fundamental difficulty in such systems is the small relative magnitude of the second term on the right-hand side of Eq. (21.5) when the coherence time of the detected field is much smaller than the detector's response time.[5]

21.3 Quantum Photon-Correlation Imaging

We now consider a light source that emits photons in pairs. The coherence properties of such light must be described using quantum coherence theory.[18] For each pair, the quantum state is

$$\left|\Psi\right\rangle = \iint d\mathbf{x}\, d\mathbf{x}'\, \psi_s(\mathbf{x},\mathbf{x}')\left|1_{\mathbf{x}},1_{\mathbf{x}'}\right\rangle, \qquad (21.6)$$

where $\psi(\mathbf{x},\mathbf{x}')$ is the two-photon wave function, i.e., the probability that the photons are emitted from positions $\mathbf{x}$ and $\mathbf{x}'$ is $\left|\psi_s(\mathbf{x},\mathbf{x}')\right|^2$. In an entangled state, $\psi_s(\mathbf{x},\mathbf{x}') = \xi_s(\mathbf{x})\delta(\mathbf{x}-\mathbf{x}')$ so that the photons are emitted from a common position, although that position is random with probability density $\left|\xi_s(\mathbf{x})\right|^2$.

Such light may be generated by spontaneous parametric downconversion (SPDC) from a thin planar nonlinear crystal. For each annihilated pump photon, a pair of photons, the signal and idler, are generated in a two-photon, or biphoton, state. In this case, the complex function $\xi_s(\mathbf{x})$ in Eq. (21.6) is proportional to the conjugate of the optical field of the pump. This spatially entangled state emerges as a result of conservation of momentum, which makes the directions of the photons anticorrelated.

If the two photons are directed through systems with impulse response functions $h_1(\mathbf{x}_1, \mathbf{x})$ and $h_2(\mathbf{x}_1, \mathbf{x})$, and directed to two detectors, as in Fig. 21.1, then it can be shown that the probability of detecting photons simultaneously with detectors at positions $\mathbf{x}_1$ and $\mathbf{x}_2$ is

$$G^{(2)}(\mathbf{x}_1, \mathbf{x}_2) = \left\langle : \hat{I}(\mathbf{x}_1)\hat{I}(\mathbf{x}_2) : \right\rangle = \left| \psi(\mathbf{x}_1, \mathbf{x}_2) \right|^2, \tag{21.7}$$

i.e., is simply the square magnitude of the two-photon wave function

$$\psi(\mathbf{x}_1, \mathbf{x}_2) = \int \xi_s(\mathbf{x}) h_1(\mathbf{x}_1, \mathbf{x}) h_2(\mathbf{x}_2, \mathbf{x}) \, d\mathbf{x}. \tag{21.8}$$

The similarity between Eq. (21.8) for the two-photon wave function $\psi(\mathbf{x}_1, \mathbf{x}_2)$ and Eq. (21.1) for the second-order coherence function $G^{(1)}(\mathbf{x}_1, \mathbf{x}_2)$ is remarkable. The source function $\xi_s(x)$ plays the role of the intensity of the incoherent source $I_s(x)$, and, except for a conjugation operation in the incoherent case [Eq. (21.1)], the impulse response functions of the optical systems play similar roles. The origin of this similarity may be attributed to the fact that both the second-order wave function and the two-photon wave function satisfy the Wolf equations.[23]

For thermal light, in accordance with the Siegert relation set forth in Eq. (21.5), the two-photon coincidence rate is proportional to $\left| G^{(1)}(\mathbf{x}_1, \mathbf{x}_2) \right|^2$, to which a background term is added, whereas in the two-photon case, the photon coincidence rate is simply $\left| \psi(\mathbf{x}_1, \mathbf{x}_2) \right|^2$. The background term, which typically dominates Eq. (21.5), as discussed earlier, is absent in the two-photon case, as was recognized by Belinskii and Klyshko.[9]

21.3.1 Ghost imaging

If the imaging configuration depicted in Fig. 21.2 is used with a two-photon source, then diffraction-limited imaging is attained if the condition

$$\frac{1}{d_2 + d_1} + \frac{1}{d_3} = \frac{1}{f} \tag{21.9}$$

is satisfied.[12] The sign change in Eq. (21.9), in comparison to Eq. (21.2), is attributed to the conjugation in the imaging equation.

21.3.2 Van Cittert–Zernike theorem

If the imaging configuration depicted in Fig. 21.3 is used with a two-photon source, which is itself the object, then the imaging equation becomes

$$G^{(1)}(\mathbf{x}_1, \mathbf{x}_2) \propto \int O(\mathbf{x}) \exp\left[-i\frac{2\pi}{\lambda f}(\mathbf{x}_2 + \mathbf{x}_1).\mathbf{x} \right] d\mathbf{x}. \qquad (21.10)$$

This equation is identical to Eq. (21.4) except for a change in sign. When measured as a function of $\mathbf{x}_1 + \mathbf{x}_2$, the coherence function $G^{(1)}$ is proportional to the Fourier transform of $O(\mathbf{x})$. For example, if $O(\mathbf{x})$ is uniform, then $G^{(1)}(\mathbf{x}_1, \mathbf{x}_2) \propto \delta(\mathbf{x}_2 + \mathbf{x}_1)$, i.e., if a photon is observed at $\mathbf{x}_1$, then another must be detected at $-\mathbf{x}_1$.

21.3.3 Quantum microscopy and lithography

The intensity correlation may be measured at the same position by making use of a single detector responsive to the rate of two-photon absorption. For two-photon light in an entangled state, $G^{(2)}(\mathbf{x}_1, \mathbf{x}_1) = |\psi(\mathbf{x}_1, \mathbf{x}_1)|^2$, with

$$\psi(\mathbf{x}_1, \mathbf{x}_1) = \int \xi_s(\mathbf{x}) h^2(\mathbf{x}_1, \mathbf{x}) \, d\mathbf{x}, \qquad (21.11)$$

in the special case when the two optical systems h_1 and h_2 collapse into a single imaging system h, as can be shown by use of Eq. (21.8). The imaging system is therefore linear with impulse response function $h^2(\mathbf{x}_1, \mathbf{x})$. For example, for a 2-*f* Fourier optics system, $h(\mathbf{x}_1, \mathbf{x})$ is given by Eq. (21.3). The squaring operation increases the frequency by a factor of two. For example, for a two-slit object, the system creates a sinusoidal pattern at twice the spatial frequency. This feature plays a role in quantum (entangled-photon) microscopy[24,25] and photoemission,[26] and is, in essence, the principle behind quantum lithography,[27] which exploits entanglement to enhance resolution. This enhancement cannot be attained by making use of a classical thermal-imaging system.

21.4 Noise in Photon-Correlation Imaging

In this section we compare the accuracy of classical and quantum imaging systems by determining the error of measurement of the photon-correlation functions in each case. It is convenient to define the normalized photon-correlation function $g^{(2)} = G^{(2)}/(I_1 I_2)$, the normalized second-order coherence function $g^{(1)} = G^{(1)}/(I_1 I_2)^{1/2}$, and the normalized two-photon wave function $\varphi = \psi/(I_1 I_2)^{1/2}$, where I_1 and I_2 are the intensities (or the mean number of photons) at the two detectors. For classical imaging, Eq. (21.5) becomes

$$g^{(2)} - 1 = \frac{1}{M} \left| g^{(1)} \right|^2, \qquad (21.12)$$

while for quantum case, Eq. (21.7) becomes

$$g^{(2)} = |\varphi|^2 . \tag{21.13}$$

The detectors measure estimates of the functions $G^{(2)}$ and I, which we label $\hat{G}^{(2)}$ and $\hat{I}$, respectively. These estimates are used to calculate estimates of $g^{(2)}$ via the relation $\hat{g}^{(2)} = \hat{G}^{(2)}/(\hat{I}_1 \hat{I}_2)$. We now proceed to determine the errors in the estimate $\hat{g}^{(2)}$ in the classical and quantum cases.

The uncertainty in the measurement of the intensity-correlation function $G^{(2)}(\mathbf{x}_1, \mathbf{x}_2) = \langle : \hat{I}(\mathbf{x}_1)\hat{I}(\mathbf{x}_2) : \rangle$ stems from the finite time available to measure the average intensity products. This function is usually measured by registering the number of photon counts n_1 and n_2 detected in each of the two detectors during a sequence of short time intervals, each of duration T, and averaging the product of the counts,[5]

$$\hat{G}^{(2)} = \frac{1}{N} \sum_{m=1}^{N} n_1(m) n_2(m) . \tag{21.14}$$

Here, the index m refers to the mth time interval and N is the total number of intervals observed. The total duration of the measurement is NT. Likewise, an estimate of the intensity is measured at each detector by computing the averages

$$\hat{I}_j = \frac{1}{N} \sum_{m=1}^{N} n_i(m), \quad i = 1, 2 . \tag{21.15}$$

Clearly, if $N \to \infty$, the measured functions $\hat{G}^{(2)}$ and $\hat{I}_i$ equal exactly the true functions $G^{(2)}$ and I_i, respectively.

The normalized measurement errors e in the classical (C) and quantum (Q) cases are defined by the following normalized variances:

$$e_C^2 = \frac{\text{Var}\{\hat{g}^{(2)}\}}{\left[g^{(2)} - 1 \right]^2}, \qquad e_Q^2 = \frac{\text{Var}\{\hat{g}^{(2)}\}}{\left[g^{(2)} \right]^2} . \tag{21.16}$$

For comparison, we define the ratio

$$R = \frac{e_C^2}{e_Q^2} . \tag{21.17}$$

If $R > 1$, then quantum imaging offers a statistical advantage, and vice versa.

Computation of the variances in Eq. (21.16) is a lengthy process, particularly in the classical case for which the photon counts obey Bose-Einstein statistics. We assume that the photon counts $n_i(m)$ are statistically independent for the different counting intervals. Since it is difficult to determine the variance of the ratio $\hat{g}^{(2)} = \hat{G}^{(2)} / (\hat{I}_1 \hat{I}_2)$, we assume that the errors are sufficiently small so that we can use the relation $1/\hat{I} \approx (1/I)[1-(\hat{I}-I)/I]$ to simplify the computation in terms of statistical moments of n_i. To further simplify the computation, we have also assumed that the thermal light in the classical case has a Lorentzian spectrum, i.e., an exponential coherence function, with coherence time τ_c. The following expressions result:

$$e_C^2 = \frac{1}{N} \frac{M^2}{\gamma^2} \left[\frac{1+g^2}{g^4} \frac{1}{\overline{n}_C^2} + \frac{2+4g^2-2g^4}{g^4} \frac{1}{\overline{n}_C} + \frac{5+10g^2-11g^4}{2g^4}\gamma \right], \quad (21.18)$$

$$e_Q^2 = \frac{1}{N} \frac{1}{g^2} \frac{1}{\overline{n}_Q^2} . \quad (21.19)$$

Here, the symbol g is used to denote $\left|g^{(1)}\right|$ or $|\varphi|$, for the classical and quantum cases, respectively, and $\overline{n}_C$ and $\overline{n}_Q$ are the mean number of photon detected in each time interval in the classical and quantum cases, respectively. The quantity M is the degrees-of-freedom parameter, which is a function of the ratio $\gamma = T/\tau_c$.

As expected, the errors e_C and e_Q depend on $\sqrt{N}$ for both cases, but the dependence on the mean number of photons, the ratio $\gamma = T/\tau_c$, and the quantity g, which is to be ultimately estimated, are different. It is useful to take the following two limiting cases:

Case 1. If the mean number of counts in both cases are equal and small, i.e., $\overline{n}_C = \overline{n}_Q \ll 1$, then

$$R = \frac{M^2}{\gamma^2} f_1(g), \quad f_1(g) = \frac{1+g^2}{g^2} . \quad (21.20)$$

The quantity R can then be substantially greater than unity, as can be seen from the plots of $f_1(g)$ and M/γ in Fig. 21.4, for thermal light with Lorenzian spectrum, for which $M = 2\gamma^2/(e^{-2\gamma} + 2\gamma - 1)$. It follows that quantum imaging can offer a significant statistical advantage under these conditions.[28,29]

Case 2. In reality, the mean number of photons in the quantum case is typically small, i.e., $\bar{n}_Q \ll 1$, since the generation of a high flux of biphotons is generally difficult. Assuming strong thermal light, i.e., $\bar{n}_C \gg 1$, we obtain the ratio

$$R = \frac{\bar{n}_Q^2}{\bar{n}_C^2} \frac{M^2}{\gamma} f_2(g), \quad f_2(g) = \frac{5 + 10g^2 - 11g^4}{2g^2} . \tag{21.21}$$

As shown in Fig. 21.4, the factor $f_2(g)$ can be large. Also, M and M/γ are greater than unity and can be large for large values of γ. These factors favor quantum imaging. However, it is the ratio of the mean counts $\bar{n}_Q/\bar{n}_C$ that can be sufficiently small, allowing classical imaging to outdo quantum imaging.
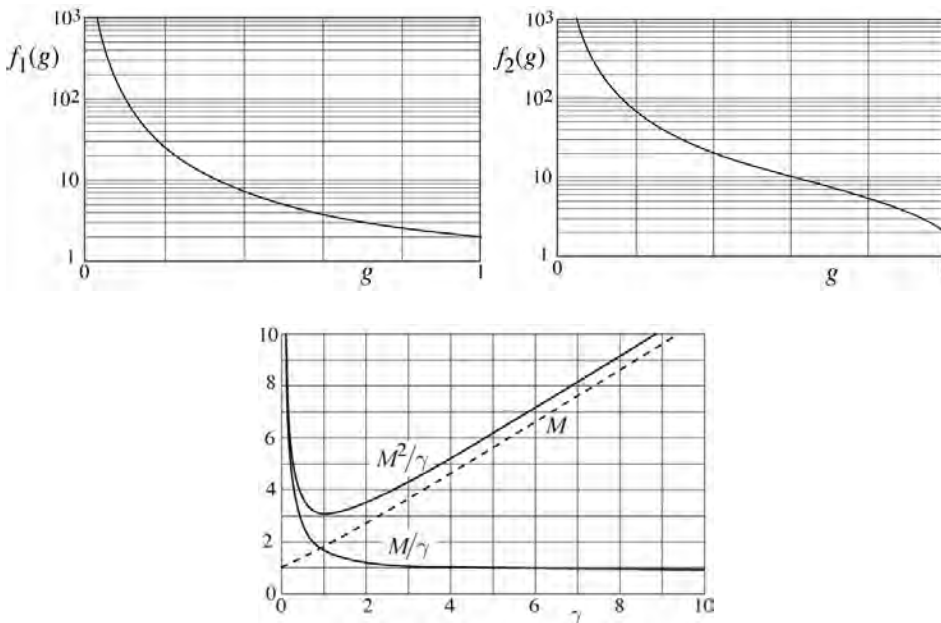

Figure 21.4 Factors affecting the error ratio R.

21.5 Conclusion

Imaging based on photon-correlation measurement with thermal light exploits the photon-bunching effect, which is accompanied by a large background. Two-photon light, on the other hand, comprises complete bunching since the photons arrive simultaneously, and it therefore offers the same possibilities for imaging without the background attendant to thermal light. Both systems offer possibilities for coherent imaging, including ghost imaging, which is *not* a unique feature of quantum imaging.[30] Because the only difference in the imaging equations is a conjugation factor, quantum imaging offers no advantage in

resolution in a configuration using two detectors. In the degenerate case for which the two detectors become one, i.e., if the detector is a two-photon absorber, the quantum paradigm offers a factor of two advantage in resolution.

The sensitivity of the classical and quantum imaging systems are, of course, different because the noises associated with the sources are different. Quantum imaging has a significantly greater signal-to-noise ratio—if the same mean number of photons are used. Because the generation of a high two-photon flux is difficult, this advantage has not yet been exploited in real imaging systems.

Acknowledgments

References

1. Barrett, H.H., and Myers, K., *Foundations of Image Science*, Wiley, Hoboken, NJ (2003).

2. Saleh, B.E.A., and Teich, M.C., *Fundamentals of Photonics*, 2nd ed., Wiley, Hoboken, NJ (2007).

3. Wolf, E., *Introduction to the Theory of Coherence and Polarization of Light*, Cambridge University Press, New York (2007).

4. Mandel, L., and Wolf, E., *Optical Coherence and Quantum Optics*, Chap. 22, Cambridge University Press, New York (1995).

5. Saleh, B.E.A., *Photoelectron Statistics*, Springer, New York (1978).

6. Hanbury-Brown, R., *The Intensity Interferometer*, Taylor & Francis, London (1974).

7. Goldberger, M.L., Lewis, H.W., and Watson, K.M., "Use of intensity correlation to determine the phase of a scattering amplitude," *Phys. Rev.,* **132**, 2764–2787, 1963.

8. Klyshko, D.N., *Photons and Nonlinear Optics*, Nauka, Moscow (1980) [Translation: Gordon and Breach, New York (1988)].

9. Belinskii, A.V., and Klyshko, D.N., "Two-photon optics: diffraction, holography, and transformation of two-dimensional signals," *Zh. Eksp. Teor. Fiz.*, **105**, 487–493, 1994 [Translation: *Sov. Phys. JETP*, **78**, 259–262, 1994].

10. Strekalov, D.V., Sergienko, A.V., Klyshko, D.N., and Shih, Y.H., "Observation of two-photon `ghost' interference and diffraction," *Phys. Rev. Lett.*, **74**, 3600–3603, 1995.

11. Pittman, T.B., Shih, Y.H., Strekalov, D.V., and Sergienko, A.V., "Optical imaging by means of two-photon quantum entanglement," *Phys. Rev. A*, **52**, R3429–R3432, 1995.

12. Pittman, T.B., Strekalov, D.V., Klyshko, D.N., Rubin, M.H., Sergienko, A.V., and Shih, Y.H., "Two-photon geometric optics," *Phys. Rev. A*, **53**, 2804–2815, 1996.

13. Saleh, B.E.A., Popescu, S., and Teich, M.C., "Generalized entangled-photon imaging," *Proc. Ninth Ann. Mtg. IEEE Lasers and Electro-Optics Society*, Vol. 1, pp. 362–363, IEEE, Piscataway, NJ (1996).

14. Abouraddy, A.F., Saleh, B.E.A., Sergienko, A.V., and Teich, M.C., "Role of entanglement in two-photon imaging." *Phys. Rev. Lett.* **87**, 123602, 2001.

15. Abouraddy, A.F., Saleh, B.E.A., Sergienko, A.V., and Teich, M.C., "Quantum holography," *Opt. Expr.,* **9**, 498–505, 2001.

16. Abouraddy, A.F., Saleh, B.E.A., Sergienko, A.V., and Teich, M.C., "Entangled-photon Fourier optics," *J. Opt. Soc. Am. B*, **19**, 1174–1184, 2002.

17. Goodman, J.W., *Introduction to Fourier Optics*, 2nd ed., Roberts and Company, Englewood (2004).

18. Glauber, R.J., "The quantum theory of optical coherence," *Phys. Rev.*, **130**, 2529–2539, 1963.

19. Saleh, B.E.A., Abouraddy, A.F., Sergienko, A.V., and Teich, M.C., "Duality between partial coherence and partial entanglement," *Phys. Rev. A*, **62**, 043816, 2000.

20. Gatti, A., Brambilla, E., Bache, M., and Lugiato, L.A., "Ghost imaging with thermal light: comparing entanglement and classical correlation," *Phys. Rev. Lett.*, **93**, 093602, 2004.

21. Gatti, A., Brambilla, E., Bache, M., and Lugiato, L.A., "Correlated imaging, quantum and classical," *Phys. Rev. A*, **70**, 013802, 2004.

22. Ferri, F., Magatti, D., Gatti, A., Bache, M., Brambilla, E., and Lugiato, L.A., "High-resolution ghost image and ghost diffraction experiments with thermal light," *Phys. Rev. Lett.*, **94**, 183602, 2005.

23. Saleh, B.E.A., Teich, M.C., and Sergienko, A.V., "Wolf equations for two photon light," *Phys. Rev. Lett.*, **94**, 223601, 2005.

24. Teich, M.C., and Saleh, B.E.A., "Entangled-photon microscopy." *Československý časopis pro fyziku* (Prague), **47**, 3–8, 1997; Teich, M.C., and Saleh, B.E.A., "Entangled-Photon Microscopy, Spectroscopy, and Display," U.S. Patent No. 5,796,477 (issued August 18, 1998).

25. Nasr, M.B., Abouraddy, A.F., Booth, M., Saleh, B.E.A., Sergienko, A.V., Teich, M.C., Kempe, M., and Wolleschensky, R., "Biphoton focusing for two-photon excitation," *Phys. Rev. A*, **65**, 023816, 2002.

26. Lissandrin, F., Saleh, B.E.A., Sergienko, A.V., and Teich, M.C., "Quantum theory of entangled-photon photoemission," *Phys. Rev. B*, **69**, 165317, 2004.

27. Boto, A.N., Kok, P., Abrams, D.S., Braunstein, S.L., Williams, C.P., and Dowling, J.P., "Quantum interferometric optical lithography: Exploiting

    entanglement to beat the diffraction limit," *Phys. Rev. Lett.*, **85**, 2733–2736, 2000.

28. Jakeman, E., and Rarity, J.G., "The use of pair production processes to reduce quantum noise in transmission measurements," *Opt. Commun.*, **59**, 219–223, 1986.

29. Hayat, M.M., Joobeur, A., and Saleh, B.E.A., "Reduction of quantum noise in transmittance estimation using photon-correlated beams," *J. Opt. Soc. Am. A*, **16**, 348–358, 1999.

30. Gatti, A., Brambilla, E., and Lugiato, L.A., "Quantum imaging," *Progress in Optics*, Vol. 51, E. Wolf, Ed., Elsevier, New York (2008).